applied sciences

MDPI

Article

Voltage Reference Realignment Cell Balance to Solve Overvoltage Caused by Gradual Damage of Series-Connected Batteries

Sang-Sun Yun [1] and Seok-Cheol Kee [2,*]

[1] Department of Smart Car Engineering, Chungbuk National University, Cheongju 28644, Republic of Korea; ssyun@avgenius.kr
[2] Department of Intelligent Systems & Robotics, Chungbuk National University, Cheongju 28644, Republic of Korea
* Correspondence: sckee@chungbuk.ac.kr; Tel.: +82-43-249-1683

Abstract: This paper analyzes the cause of electric vehicle battery fires. The fundamental cause is attributed to a low cell balance current, and it is proven that the variation in the battery's internal voltage due to temperature change is the decisive reason for battery fires. In this paper, the authors studied a method of solving the problem by changing only the software of the existing Battery Management System (BMS) without changing the hardware. Batteries cannot be made with 100% capacity, resulting in voltage division. Cell balancing is performed to prevent such phenomena, but a low cell balance current prevents the proper operation of cell balancing. As a result, relatively small batteries, due to progressive degradation, have continuous voltage rise toward overvoltage. Subsequently, an additional voltage rise occurs as the chemical activity of the battery increases due to temperature rise. In this paper, a new cell balancing method is proposed to limit the aging process of cells with a relatively small capacity and peak voltage. In addition, it was validated through simulation using MATLAB R2019a.

Keywords: battery fire; battery aging; allowed capacity deviation; series-connected battery; chemical reaction activity

Citation: Yun, S.-S.; Kee, S.-C. Voltage Reference Realignment Cell Balance to Solve Overvoltage Caused by Gradual Damage of Series-Connected Batteries. *Appl. Sci.* **2023**, *13*, 7624. https://doi.org/10.3390/app13137624

Academic Editors: Desmond Gibson, Mojtaba Mirzaeian, Peter Hall and Saule Aidarova

Received: 19 May 2023
Revised: 25 June 2023
Accepted: 26 June 2023
Published: 28 June 2023

1. Introduction

The emergence of lithium-ion batteries, which have high energy density, has enabled the popularization of batteries. This has allowed for their application in various fields, and they have been widely adopted in society. However, there is a lack of research on the fundamental causes of battery fires.

1.1. Series Connection of Batteries

When series-connected batteries are charged from a source, a voltage distribution occurs across each battery [1–21]. When 100% capacity is equal, the voltage is evenly distributed. However, it is impossible to produce batteries with 100% identical capacity in mass production. In fact, with series-connected batteries, the voltage is not evenly distributed across each battery. That is, different batteries have different charging voltages. Additionally, each change in the capacity of series-connected batteries with a single current loop also represents a different charging rate. Batteries with relatively small capacities quickly rise in the state of charge (SOC). Conversely, batteries with relatively large capacities have a slow rise in the SOC. The case of discharge is similar [15–22]. Different SOCs have different Direct Current Internal Resistances (DCIRs) [22–38]. This causes a large potential difference between each battery. In this way, each battery repeats charging and discharging under different conditions.

1.2. Differentiated Progressive Damages

Of course, the rate of aging proceeds differently [7,30–38]. As this phenomenon is repeated, the aging of a battery with a relatively small capacity is accelerated. Most vehicle battery fires occur while charging or after charging is complete [39–46]. Most of the battery fires of large-capacity Energy Storage Systems (ESSs) occurred during the dormant period. An electric vehicle fire case was studied in "Effect of Capacity Variation in Series-Connected Batteries on Aging" [7]. The case of a large-capacity ESS was studied in "Energy Storage System Safety Operation Plan by Preventing Overcharge During Relaxation Time" [45]. In both cases, there was no problem at the beginning of mass production, but a fire occurred during use. That is, a fire was caused by progressive damage. The fire occurred because the cell balance did not properly work in the process of repeated charging and discharging. As the battery capacity increased, the cell balance current also had to increase [47–50].

However, the increase in cell balance current caused high temperature heating and caused the Battery Management System (BMS) to malfunction. The research on increasing the cell balancing current was discontinued in the past because no major issues were found with a low cell balancing current. In addition, the BMS still maintains the cell balance at around 100 mA. However, if progressive damage occurs and accumulates over time, it can lead to a fire. The purpose of this paper is to address the fundamental cause of electric vehicle battery fires and find a solution that can be directly applied to existing BMSs. The cause of electric vehicle battery fires can occur due to fundamental and decisive factors, and, in Section 2, simulation comparison data for the fundamental causes are obtained, and experimental data on voltage changes in batteries due to temperature fluctuations, a decisive factor, are mentioned. Section 3 describes the proposed cell balancing method and obtains simulation results. In Section 4, the existing simple voltage-based cell balance method and the proposed cell balance method are compared and analyzed. In Section 5, the conclusion of this study and future research goals are mentioned. The purpose of this paper is to study a new cell balancing method that limits the occurrence of overvoltage in batteries with a relatively small capacity due to the progressive damage of series-connected batteries.

2. Overvoltage of a Battery

The one-time charge usage time was extended due to user demand, resulting in an increase in battery capacity over time. However, the cell balancing current remained at around 100 mA due to the occurrence of high temperatures. In the past, the problem of a low cell balancing current was not considered significant. However, this section explains that it contributes to the cause of battery fires in series-connected batteries.

The currently developed BMSs are designed to protect the battery from external factors such as overvoltage, overcurrent, and high temperatures. However, they are vulnerable to voltage increases caused by the battery's structure or in the battery itself. This section explains the battery's structure and the voltage increase caused by temperature changes.

2.1. Problem of Low Cell Balancing Current

Cell balance can be performed by the user at any time [12,15–18,47–50]. In particular, cell balancing during charging requires special attention. In series-connected batteries, cell balancing during charging reduces the total resistance value by connecting a resistor in parallel with the battery. As a result, the value of the overall voltage distribution of series-connected batteries is different. This section compares how a low cell balance current affects the cell balance as a function of the voltage difference with and without the cell balance.

2.1.1. In the Case of Having Cell Balancing and in the Case of Not Having It

The authors conducted simulations for four series-connected batteries with and without cell balancing. Bat #1, Bat #2, Bat #3, and Bat #4 were set to 60 Ah, 59.4 Ah, 60.6 Ah, and 60 Ah, respectively, assuming a battery tolerance of $\pm 1\%$. Figure 1a shows the simulation model with and without cell balancing. Figure 1b shows the battery aging settings, where all aging cycle variables for the batteries are the same, except for the values related to capacity, which differ according to the settings. The batteries in Figure 1 use the lithium-ion battery library provided by MATLAB R2019a, and the CC-CV battery charger library also provided by MATLAB R2019a was used.

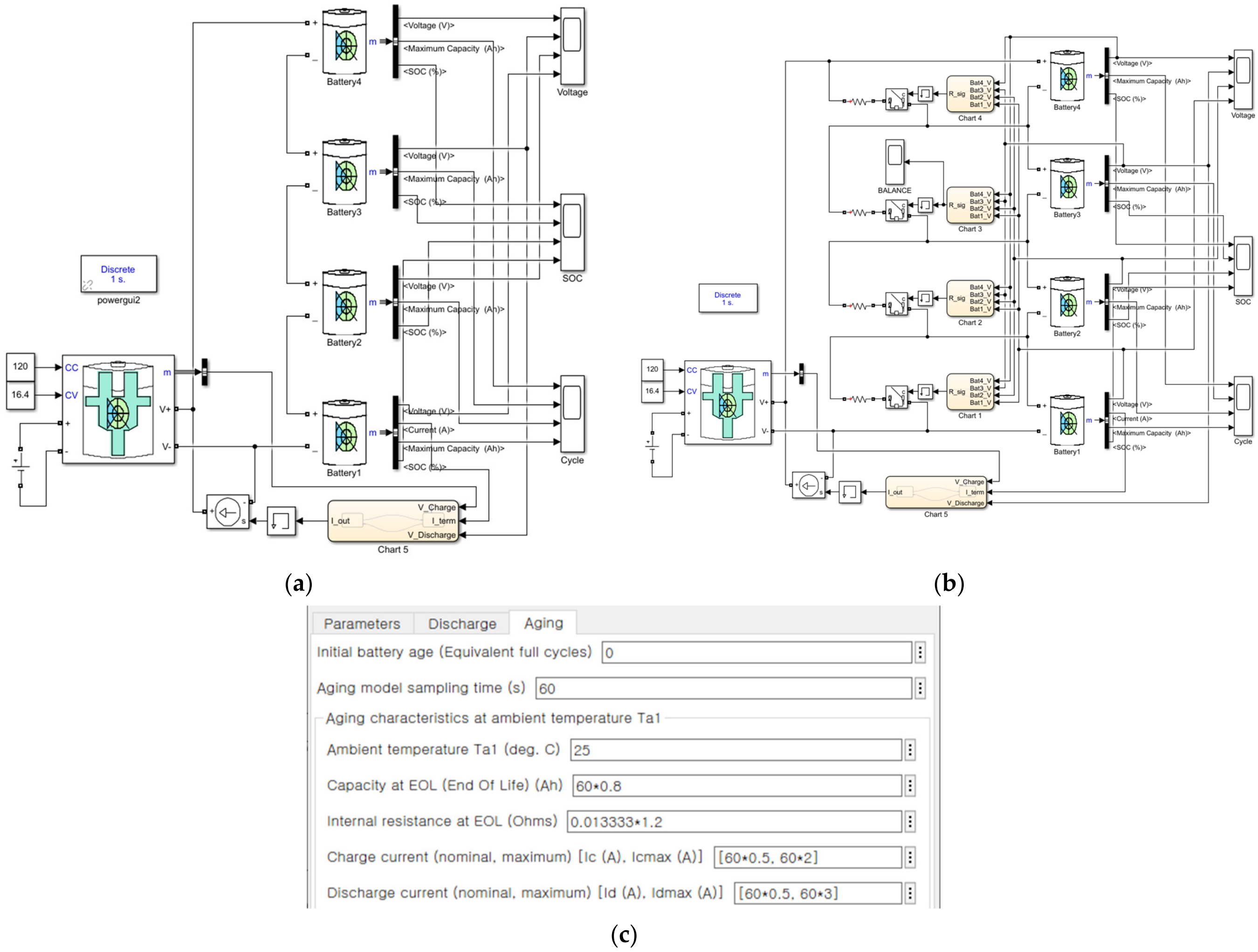

Figure 1. Serial battery simulation. (**a**) Serial-connected model; (**b**) with cell balance model; (**c**) battery aging settings.

Figure 2 shows the Stateflow for the chart shown in Figure 1. Figure 2a shows the Stateflow applied to Charts #1, #2, #3, and #4, which demonstrates a simple voltage comparison cell balancing method commonly used in the industry. Cell balancing is activated when a voltage difference of 30 mV or more is detected among the batteries and stops when the voltage difference decreases to 10 mV or less. Figure 2b shows the Stateflow for Chart #5, which illustrates the conditions for charging and discharging. Charging was performed at 2 C and ended at 0.5 C in the constant voltage (CV) region, while discharging was performed at 2 C.

Figure 3 shows the simulation results of Figure 1, where (a) shows the voltage results and (b) shows the SOC results. The difference between the cases with and without cell balancing cannot be easily observed due to a low cell balance. In Figure 3a, it was confirmed that the voltage of Bat #3 was the highest during charging and the lowest during discharging. This phenomenon was explained in the paper "Effect of capacity variation in series-connected batteries on aging" as occurring because the discharge and charge of relatively smaller batteries occur relatively quickly.

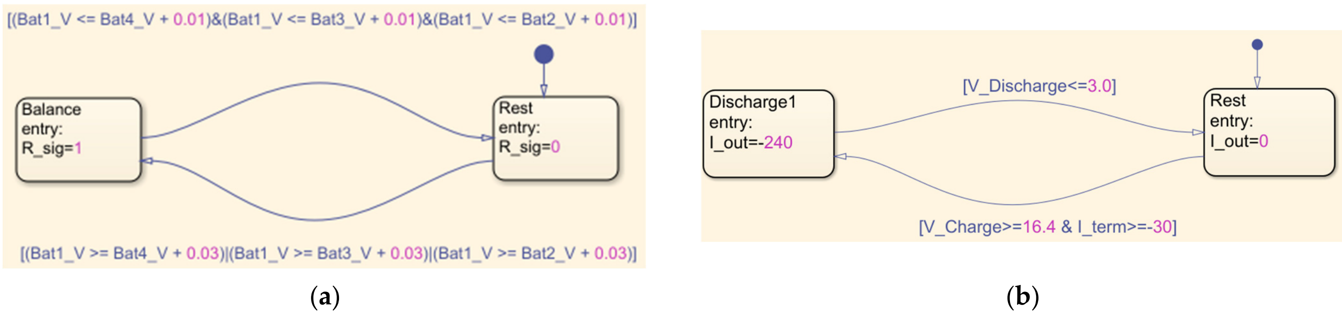

Figure 2. Stateflow of chart in Figure 1a. (**a**) Charts #1, #2, #3, and #4; (**b**) chart #5.

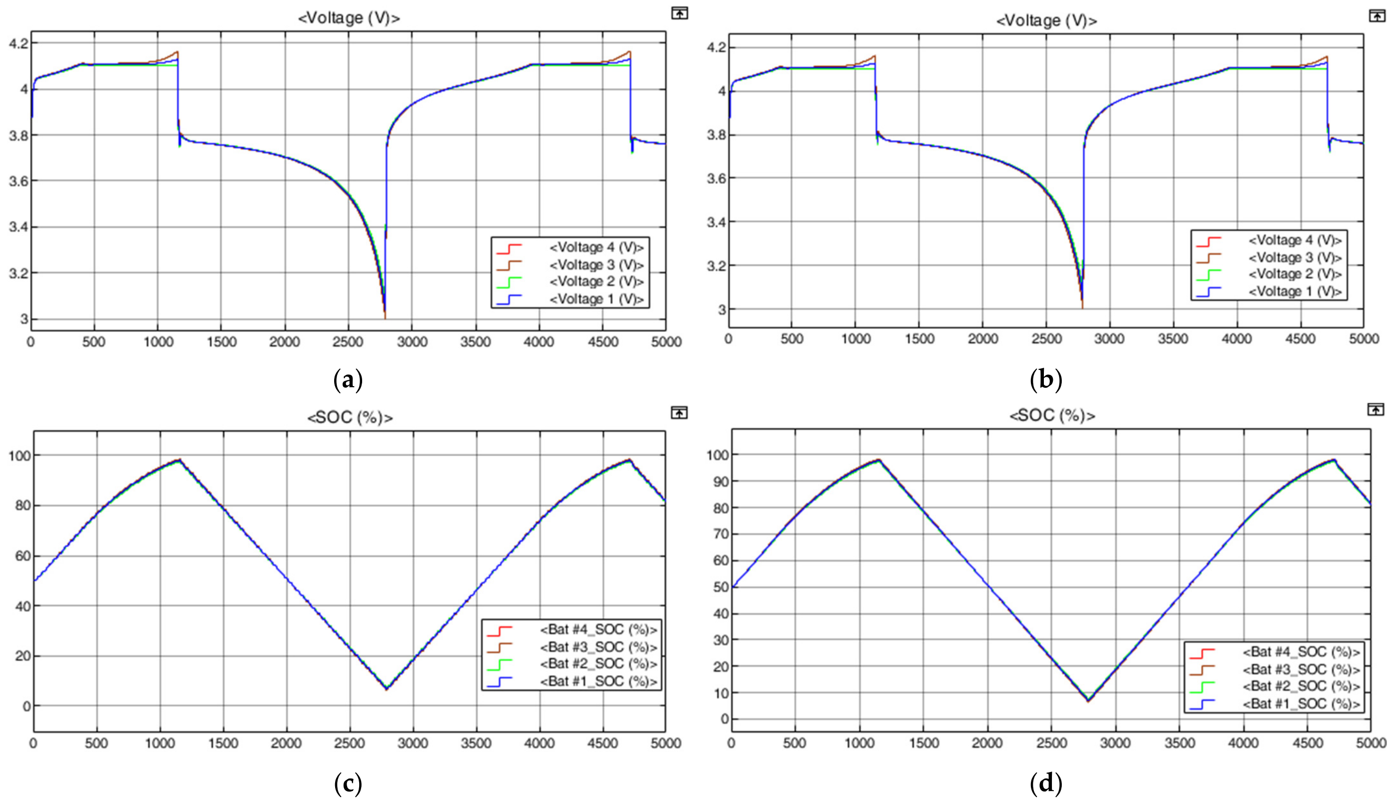

Figure 3. One cycle of simulation results. (**a**) Serial-connected voltage; (**b**) with cell balance voltage; (**c**) serial-connected SOC; (**d**) with cell balance SOC.

During the constant current (CC) charging phase, if the ideal capacity of the batteries is the same, the voltage of each battery should be equally distributed, as shown in Equation (1).

$$V_{bat1} = V_{bat2} = V_{bat3} = V_{bat4} \tag{1}$$

However, if there is a deviation in the battery capacity, as shown in Figure 3, Equation (2) applies. In Equation (2), the initial voltage of each battery is different, there is no voltage limit during the CC phase, and the rise in voltage is determined by the internal resistance of each battery because the charging current is the same for all batteries.

$$V'_{bat1} = V_{bat1} + I_{CC} \times R_{bat1},\ V'_{bat2} = V_{bat2} + I_{CC} \times R_{bat2},\ V'_{bat3} = V_{bat3} + I_{CC} \times R_{bat3},\ V'_{bat4} = V_{bat4} + I_{CC} \times R_{bat4}$$
$$V'_{bat\#n}\text{: each battery's charging voltage; } V_{bat\#n}\text{: each battery's initial charging voltage;} \tag{2}$$
$$I_{CC}\text{: steady-state current of the constant current region; } R_{bat\#n}\text{: the DCIR for each battery's SOC.}$$

During the CV phase that follows, voltage redistribution occurs due to the voltage limit of the charging voltage and the different SOCs, as shown in Equation (3).

$$
\begin{gathered}
V_{CV} = V_{bat1} + V_{bat2} + V_{bat3} + V_{bat4} \\
V_{CV} = (1/4 \times V_{CV} + I_{CV} \times R_{bat1}/R_{total} - 1/4 \times I_{CV} \times R_{total}) + \\
(1/4 \times V_{CV} + I_{CV} \times R_{bat2}/R_{total} - 1/4 \times I_{CV} \times R_{total}) + \\
(1/4 \times V_{CV} + I_{CV} \times R_{bat3}/R_{total} - 1/4 \times I_{CV} \times R_{total}) + \\
(1/4 \times V_{CV} + I_{CV} \times R_{bat4}/R_{total} - 1/4 \times I_{CV} \times R_{total}), \\
V_{bat1} - 1/4 \times V_{CV} = (I_{CV} \times R_{bat1}/R_{total} - 1/4 \times I_{CV} \times R_{total}) \\
= I_{CV} \times (R_{bat1} - 1/4 \times R_{total}^{2})/R_{total}, \\
V_{bat2} - 1/4 \times V_{CV} = I_{CV} \times (R_{bat2} - 1/4 \times R_{total}^{2})/R_{total}, \\
V_{bat3} - 1/4 \times V_{CV} = I_{CV} \times (R_{bat3} - 1/4 \times R_{total}^{2})/R_{total}, \\
V_{bat4} - 1/4 \times V_{CV} = I_{CV} \times (R_{bat4} - 1/4 \times R_{total}^{2})/R_{total} \\
V_{CV}\text{: charger's target charging voltage;} \\
I_{CV}\text{: changing current in the constant voltage region;} \\
R_{total}\text{: the total DCIR of series-connected batteries.}
\end{gathered} \tag{3}
$$

Table 1 summarizes the simulation results of Figure 3. Although our goal was to charge the four batteries to the same voltage, voltage distribution occurred due to the capacity variation among the batteries. At the end of charging the series-connected batteries, the highest voltage was observed in the relatively smaller Bat #3, and the lowest voltage was observed in the relatively larger Bat #2, with a voltage difference of 50 mV between the batteries. In the next section, the authors investigate the impact of different charging conditions on aging.

Table 1. Single-cycle simulation results with an allowable capacity deviation of ±1%.

Parameter		Bat #1	Bat #2	Bat #3	Bat #4
Series connected	Max. Volt.	4.128 V	4.105 V	4.165 V	4.128 V
	Min. Volt.	3.039 V	3.077 V	2.996 V	3.039 V
	Max. SOC	98.00%	97.53%	98.49%	98.00%
	Min. SOC	6.85%	7.28%	6.41%	6.85%
With cell balance	Max. Volt.	4.130 V	4.105 V	4.165 V	4.130 V
	Min. Volt.	3.047 V	3.084 V	2.999 V	3.047 V
	Max. SOC	98.02%	97.54%	98.48%	98.02%
	Min. SOC	6.96%	7.38%	6.45%	6.96%

2.1.2. Aging Progression with and without Cell Balancing

Figure 4 shows the aging simulation results of Figure 1. Even in the aging simulation, the authors could not find significant differences due to the low current of the cell balancing. The voltage results without cell balancing are shown in Figure 4a, while Figure 4b shows the voltage results with cell balancing. There is no significant difference in the progression of aging between the two simulation results. Figure 4c,d compare the voltage results in an enlarged voltage range of 4.0–4.3 V. It can be observed that, due to the low cell balancing current, cell balancing actually results in a greater increase in the maximum voltage during the aging process.

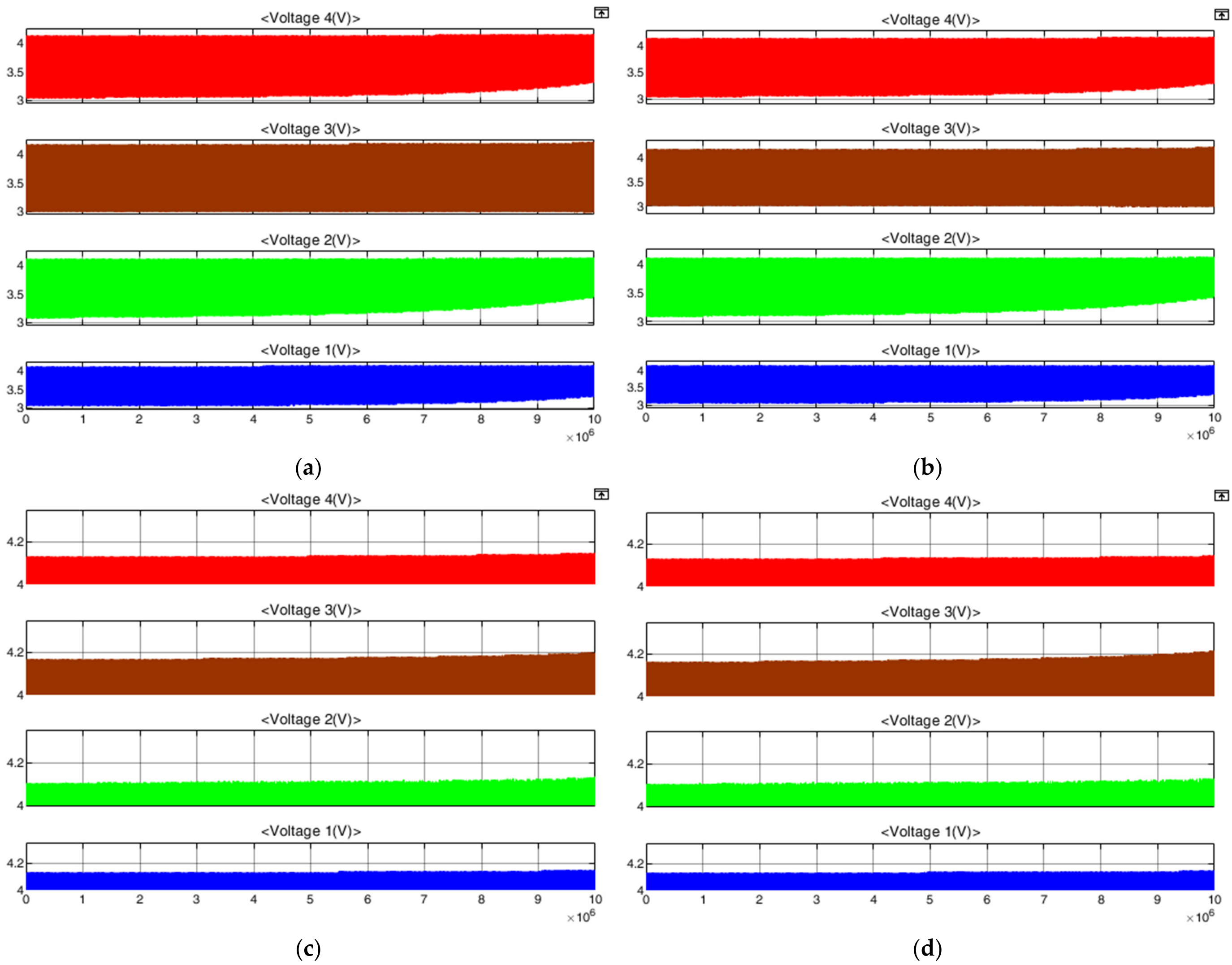

Figure 4. Voltage results of serial battery aging simulation. (**a**) Serial-connected; (**b**) with cell balance; (**c**) expanded results of serial-connected; (**d**) expanded results with cell balance.

Figure 5 shows simulation results that investigate the impact of aging on the state of charge (SOC). It can be observed that Bat #2, which has a relatively large capacity, experiences a reduction in its usable range as aging progresses. In contrast, Bat #3, which has a relatively small capacity, experiences an increase in its usable range. It can be inferred that batteries with larger capacities experience a slower progression of aging as their usable range decreases over time.

Figure 6 shows the simulation results that observe the change in the state of health (SOH) during the aging process. No significant difference was observed in the two simulation results for the SOH.

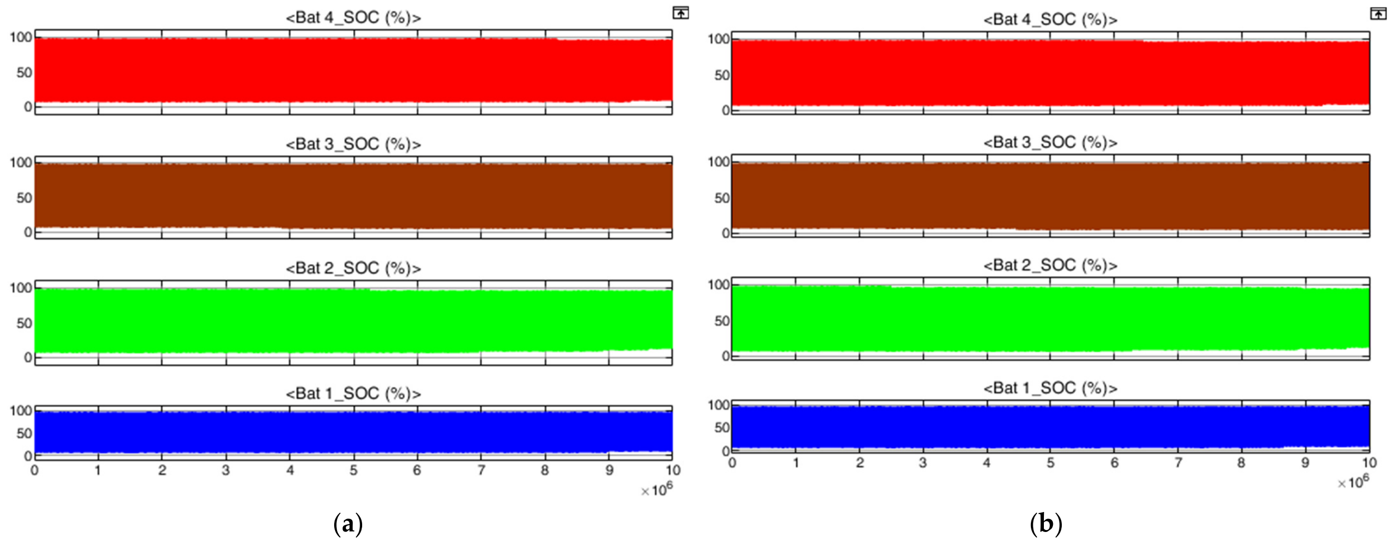

Figure 5. SOC results of serial battery aging simulation. (**a**) Serial-connected; (**b**) with cell balance.

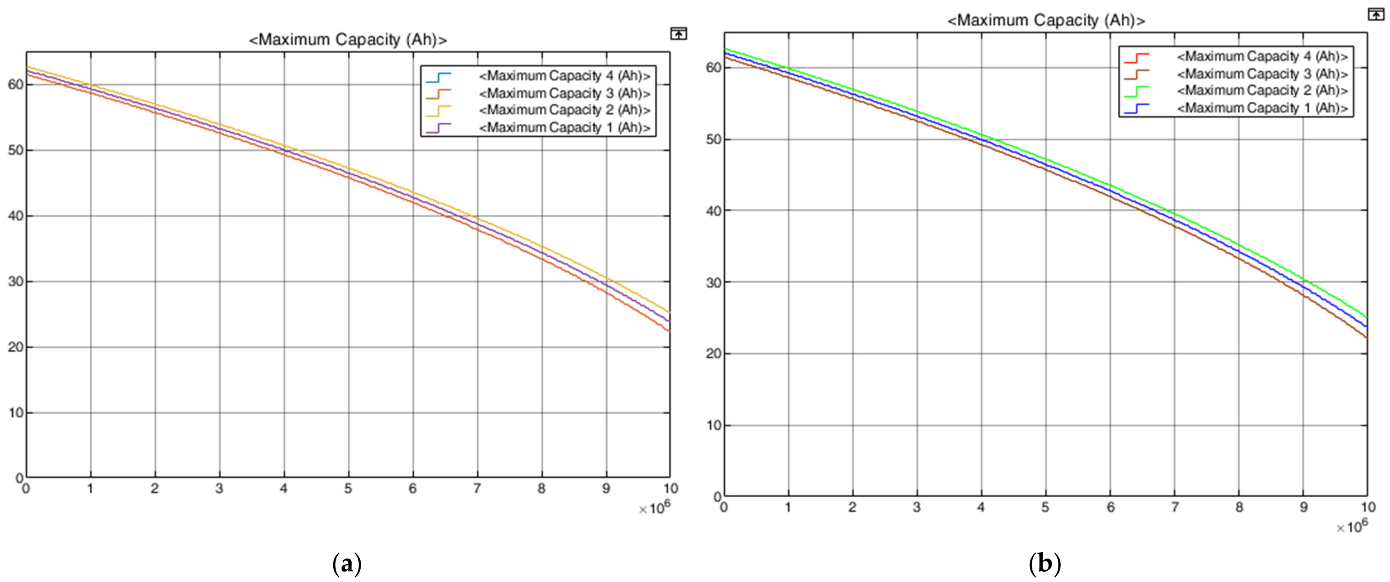

Figure 6. SOH results of serial battery aging simulation. (**a**) Serial-connected; (**b**) with cell balance.

Table 2 summarizes the results of the aging simulation. The maximum voltage without cell balance was 4.198 V, compared to 4.213 V with cell balance. This shows that a low cell balance current has a negative effect on the overvoltage caused by the voltage distribution. In addition, the SOH of the battery was relatively quickly degraded in both cases.

Table 3 presents the simulation results with a ±2% variation in the battery capacity under the same conditions. The effect of cell balancing was found to be negligible during aging. However, it was observed that there was an impact on the maximum voltage at full charge as aging progressed. In Table 2, the maximum voltage of Bat #3 increased by 48 mV from 4.165 V to 4.213 V after aging. In Table 3, after the same duration of aging, the maximum voltage of Bat #3 increased by 72 mV from 4.203 V to 4.275 V. Additionally, by examining the range of SOC usage, it was found that 93.16% was used in Table 2, while 94.14% was used in Table 3. Consequently, the maximum SOC difference increased from 2.84% to 5.06%. The SOC difference in series-connected batteries leads to voltage redistribution in the CV region due to their different DCIRs [7].

Table 2. Aging simulation results with allowable capacity deviation of ±1%.

For 10×10^6 s

Parameter		Serial Connected				With Cell Balance			
		Bat #1	**Bat #2**	**Bat #3**	**Bat #4**	**Bat #1**	**Bat #2**	**Bat #3**	**Bat #4**
Voltage (V)	Min	3.039	3.077	2.996	3.039	3.047	3.084	2.999	3.047
	Max	4.128	4.105	4.165	4.128	4.129	4.105	4.165	4.129
SOC (%)	Min	6.85	7.28	6.41	6.85	6.96	7.38	6.45	6.96
	Max	97.99	97.51	98.47	97.99	98.00	97.53	98.48	98.00
SOH (Ah)	Max	62.04	62.66	61.42	62.04	62.04	62.66	61.42	62.04
Time (Cycles)		1 Cycle				1 Cycle			
Voltage (V)	Min	3.312	3.439	2.984	3.312	3.300	6.85	96.01	9.04
	Max	4.147	4.117	4.198	4.147	4.144	4.128	4.213	4.144
SOC (%)	Min	9.04	13.00	4.23	9.04	8.76	12.37	4.30	8.76
	Max	96.01	95.00	97.14	96.01	95.92	94.62	97.46	95.92
SOH (Ah)	Max	23.63	25.05	21.12	23.63	23.54	24.94	22.02	23.54
Time (Cycles)		4170 Cycles				4176 Cycles			

Table 3. Aging simulation results with allowable capacity deviation of ±2%.

For 10×10^6 s

Parameter		Serial Connected				With Cell Balance			
		Bat #1	**Bat #2**	**Bat #3**	**Bat #4**	**Bat #1**	**Bat #2**	**Bat #3**	**Bat #4**
Voltage (V)	Min	3.077	3.144	2.996	3.077	3.080	3.150	2.998	3.080
	Max	4.123	4.102	4.204	4.123	4.123	4.102	4.203	4.123
SOC (%)	Min	7.36	8.19	6.49	7.36	7.40	8.30	6.52	7.40
	Max	97.90	96.96	98.88	97.90	97.90	96.97	98.87	97.90
SOH (Ah)	Max	62.04	63.28	60.80	62.04	62.04	63.28	60.80	62.04
Time (Cycles)		1 Cycle				1 Cycle			
Voltage (V)	Min	3.456	3.562	2.992	3.456	3.442	3.552	3.000	3.442
	Max	4.137	4.115	4.252	4.137	4.131	4.113	4.275	4.131
SOC (%)	Min	13.77	20.08	4.34	13.77	13.21	19.38	4.41	13.21
	Max	95.80	93.91	98.13	95.80	95.61	93.49	98.55	95.61
SOH (Ah)	Max	24.16	26.85	21.13	24.16	24.15	26.83	21.13	24.15
Time (Cycles)		4230 Cycles				4226 Cycles			

Table 4 shows the simulation results for a serially connected battery with an allowable capacity deviation of ±3%. During the experiment, it was found that the maximum voltage of Bat #3 exceeded the overvoltage protection (OVP) reference voltage of 4.3 V during the charge and discharge cycles. As the allowable capacity deviation increased, the energy required for cell balancing also increased. The effect of balancing was reduced due to the low cell balance current, making it difficult to distinguish the difference in the aging rate between cases with and without cell balancing.

Table 4. Aging simulation results with allowable capacity deviation of ±3%.

For 10×10^6 s

Parameter		Serial Connected				With Cell Balance			
		Bat #1	**Bat #2**	**Bat #3**	**Bat #4**	**Bat #1**	**Bat #2**	**Bat #3**	**Bat #4**
Voltage (V)	Min	3.112	3.200	2.996	3.112	3.115	3.206	2.998	3.115
	Max	4.114	4.099	4.245	4.114	4.114	4.009	4.243	4.114
SOC (%)	Min	7.87	9.10	6.57	7.87	7.91	9.20	6.60	7.91
	Max	97.74	96.35	99.22	97.74	97.75	96.36	99.21	97.75
SOH (Ah)	Max	62.04	63.90	60.18	62.04	62.04	63.90	60.18	62.04
Time (Cycles)		1 Cycle				1 Cycle			
Voltage (V)	Min	3.536	3.620	2.998	3.536	3.527	3.614	2.984	3.527
	Max	4.125	4.112	4.309	4.125	4.122	4.115	4.331	4.122
SOC (%)	Min	8.48	10.99	5.59	8.48	17.74	25.39	4.29	17.74
	Max	97.04	95.18	99.11	97.04	95.22	92.42	99.39	95.22
SOH (Ah)	Max	24.67	28.51	20.09	24.67	24.66	28.51	20.09	24.66
Time (Cycles)		4297 Cycles				4296 Cycles			

2.1.3. Comparison of Simulation Results for the Influence of Low Cell Balancing

In this session, the simulation results were compared (see Table 5). It was observed that the maximum voltage of Bat #3 increased more with a lower cell balance current than when there was no cell balance. This phenomenon can be attributed to the increased range of SOC usage, as indicated by the experimental results. Additionally, it was confirmed that as the allowable capacity deviation increased, the maximum voltage of Bat #3 even more significantly increased. This was because the difference in SOC usage range increased due to the increase in the allowable capacity deviation, resulting in an increase in the DCIR difference and voltage redistribution, which in turn increased the voltage difference between each battery [51].

Table 5. Comparison of results with and without cell balancing.

For 10×10^6 s

Parameter		Bat #1	Bat #2	Bat #3	Bat #4
Series-connected capacity deviation ±1%	Max. Volt.	↑ 0.019 V	↑ 0.012 V	↑ 0.033 V	↑ 0.019 V
	SOC Use	91.14% → 86.97%	90.23% → 82.05%	92.06% → 92.91%	91.14% → 86.97%
	SOH	↓ 61.91%	↓ 60.02%	↓ 65.61%	↓ 61.91%
	Cycles	4170 Cycles			
With cell balance capacity deviation ±1%	Max. Volt.	↑ 0.015 V	↑ 0.023 V	↑ 0.048 V	↑ 0.015 V
	SOC Use	91.04% → 87.16%	90.15% → 82.25%	92.03% → 93.16%	91.04% → 87.16%
	SOH	↓ 62.06%	↓ 60.20%	↓ 64.15%	↓ 62.06%
	Cycles	4176 Cycles			
Series-connected capacity deviation ±2%	Max. Volt.	↑ 0.014 V	↑ 0.013 V	↑ 0.048 V	↑ 0.014 V
	SOC Use	90.54% → 82.03%	88.77% → 73.83%	92.40% → 93.80%	90.54% → 82.03%
	SOH	↓ 61.06%	↓ 57.57%	↓ 65.25%	↓ 61.06%
	Cycles	4230 Cycles			
With cell balance capacity deviation ±2%	Max. Volt.	↑ 0.008 V	↑ 0.011 V	↑ 0.072 V	↑ 0.008 V
	SOC Use	90.50% → 82.40%	88.67% → 74.11%	92.35% → 94.14%	90.50% → 82.40%
	SOH	↓ 61.07%	↓ 57.60%	↓ 65.25%	↓ 61.07%
	Cycles	4226 Cycles			
Series-connected capacity deviation ±3%	Max. Volt.	↑ 0.011 V	↑ 0.013 V	↑ 0.064 V	↑ 0.011 V
	SOC Use	89.87% → 88.56%	87.25% → 84.19%	92.65% → 93.52%	89.87% → 88.56%
	SOH	↓ 60.27%	↓ 55.38%	↓ 66.62%	↓ 60.27%
	Cycles	4297 Cycles			
With cell balance capacity deviation ±3%	Max. Volt.	↑ 0.008 V	↑ 0.016 V	↑ 0.088 V	↑ 0.008 V
	SOC Use	89.84% → 77.48%	87.16% → 67.03%	92.61% → 95.10%	89.84% → 77.48%
	SOH	↓ 59.25%	↓ 55.38%	↓ 66.62%	↓ 59.25%
	Cycles	4296 Cycles			

2.2. Chemical Reaction of a Battery

Batteries are components that charge and discharge electrical energy through chemical reactions. The activity of the reaction changes with the temperature. To determine whether changes in the activity of the chemical reaction affect the voltage of the battery, experiments and simulations were conducted. The configuration of the equipment was as follows [51].

- Battery test system: MACCOR 4000 Series
- Chamber: JEIO Tech TH-G
- Digital recorder: YOKOGAWA MV1000
- Battery: Polymer Li-ion Recharged Battery DTP 6565294 (3.7 V/4000 mAh)

The following information is based on the specifications listed in the detailed product specification sheet for the battery and was used as the basis for the charging and discharging conditions [51].

- Charge limited voltage: 4.20 V
- Discharge cut-off voltage: 2.75 V
- End of charge current: 0.01 C
- Standard charge: 0.2 C (800 mA)
- Standard discharge: 0.2 C (800 mA)
- Operating temperature range:

  Charge: 10~45 °C
  Discharge: −20~60 °C

- Storage temperature range: 10~45 °C
- Operating and storage humidity range: 65 ± 20% RH

This study was conducted by reanalyzing past experimental data and discovering new facts to write about.

In the Case of Having Cell Balancing and in the Case of Not Having It

Table 6 summarizes the experimental results for the temperature-dependent voltage changes observed after performing a full charge and then varying the temperature. The range of temperature changes was based on the operating temperature range allowed by the BMS for automotive use, and voltage changes were accordingly observed. The largest voltage change occurred when the battery was charged at room temperature (25 °C) and then subjected to temperatures of −20 °C and 55 °C, resulting in a voltage change of 18 mV. It was noticed that the largest increase in the chemical reaction activity occurred when the battery was charged at room temperature and then, after complete charging, the temperature was increased to 55 °C, resulting in the influx of thermal energy.

Table 6. After complete charging, voltage variation due to temperature.

Charge: 4.2 V/0.5 C, End of charge: 4.2 V/0.05 C

After End of Charging	Charging @ −20 °C	Charging @ 0 °C	Charging @ 25 °C	Charging @ 55 °C
Voltage (V) @ 55 °C	4.081	4.132	4.168	4.166
Voltage (V) @ −20 °C	4.074	4.124	4.150	4.154
Voltage deviation (mV)	7	8	18	12

In Table 7, experiments were conducted to observe the voltage changes with temperature variations for each SOC. The charging temperature was based on room temperature, and the charging termination condition was divided into each percentage based on the fully charged Ah. In the experimental results, the voltage change was the smallest, 1 mV, with temperature variations from −20 to 55 °C at SOC 40%. In addition, the voltage change was the largest, 32 mV, with temperature variations at SOC 0%. Such voltage changes also occurred even in the case of SOC 100%, showing a voltage change of 18 mV.

Table 7. Voltage variation due to temperature by SOC after charging at room temperature.

Charge: 4.2 V/0.5 C, End of charge: 4.2 V/0.05 C

Parameter	SOC 0%	SOC 20%	SOC 40%	SOC 60%	SOC 80%	SOC 100%
Max. voltage (V)	3.140	3.485	3.675	3.849	4.042	4.168
Min. voltage (V)	3.108	3.463	3.674	3.835	4.035	4.150
Voltage deviation (mV)	32	22	1	14	7	18

Figure 7 is a diagram that estimates the cause of the voltage change based on the experimental results of Table 7. Using the SOC–OCV graph as a reference, the solid line represents the activity change in chemical reactions due to the heat energy input into the battery caused by temperature changes. The resulting voltage change is represented by the dotted line. It can be confirmed that open-circuit voltage (OCV) changes are more pronounced near SOC 0% or 100% than the nominal voltage.

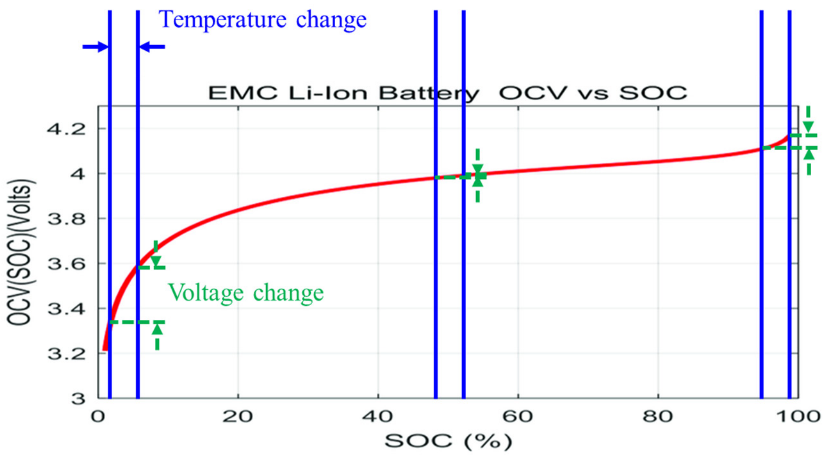

Figure 7. Voltage change according to the change in chemical reaction activity.

Based on the previous experiment, a simulation was conducted by observing the voltage change after changing the temperature from room temperature to 60 °C. Figure 8a shows the simulation model, Figure 8b shows Chart 1's flowchart, and Figure 8c shows Chart 2's flowchart. Figure 8d presents the simulation results for the battery's voltage and current, while Figure 8e displays the simulation results for the battery's state of charge (SOC). The temperature was changed from 25 °C to 60 °C at 9×10^4 s, and an increase in voltage can be observed in Figure 8c. However, Figure 8d indicates no change in the SOC, suggesting that no external charging occurred.

Table 8 summarizes the simulation results before and after the temperature changes in Figure 8 after a full charge. The voltage increased by 113 mV due to the temperature change from room temperature to 60 °C. This is thought to be due to the difference in the SOC–OCV curve of the simulation model, resulting in a larger voltage change.

Table 8. Simulation results of voltage variation according to temperature change.

State	Time (s)	Voltage (V)	SOC (%)
Temp. 25 °C	0.6×10^4 s	4.193	100
Temp. 60 °C	1.2×10^4 s	4.306	100

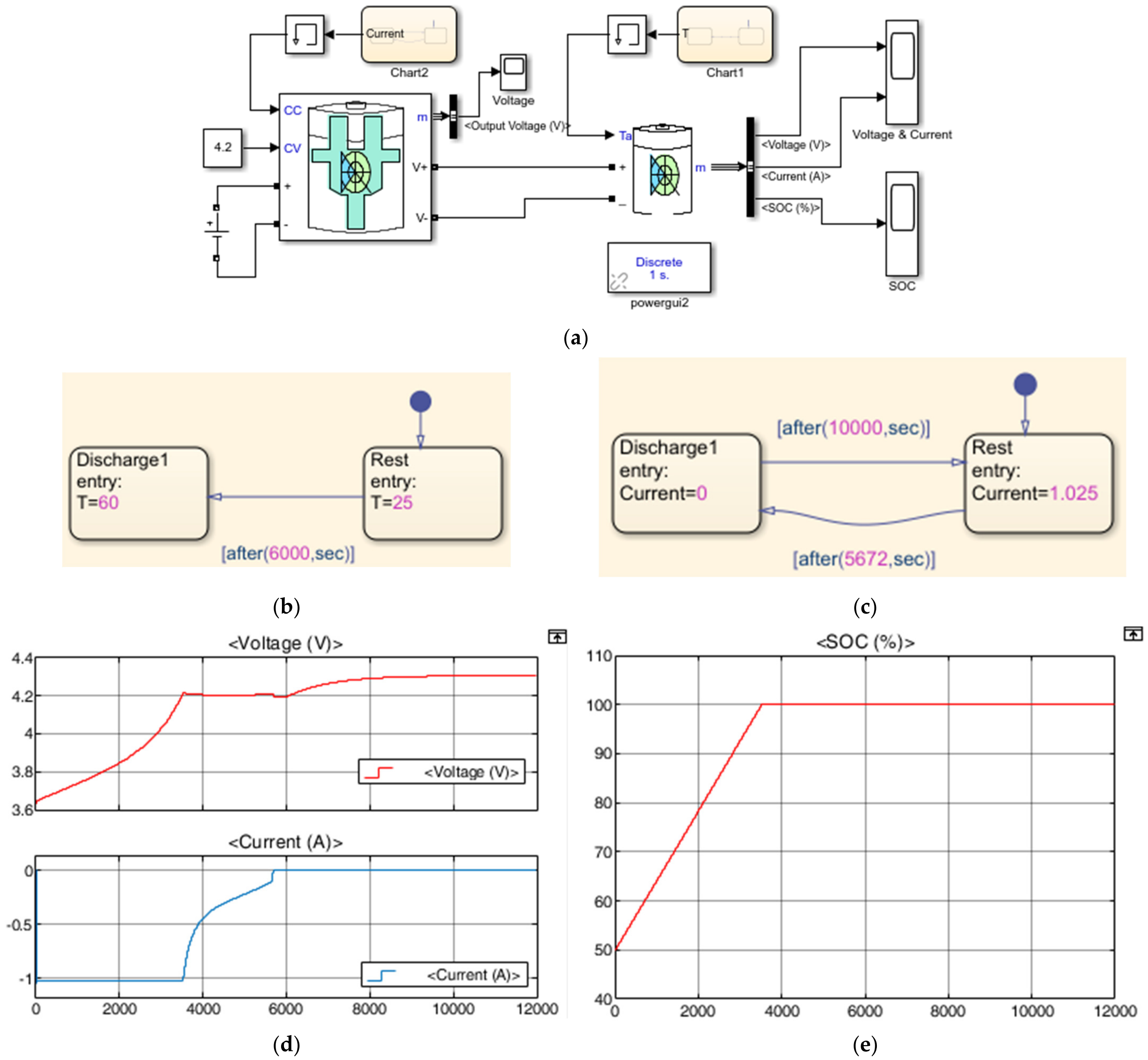

Figure 8. Environmental temperature change simulation. (**a**) Model; (**b**) Stateflow of Chart #1; (**c**) Stateflow of Chart #2; (**d**) voltage results; (**e**) SOC results.

2.3. Summary of Battery Overvoltage Generation

Sections 2.1 and 2.2 describe two factors that contribute to battery fires in electric vehicles. After charging is completed, electric vehicles forcibly terminate cell balancing, which creates conditions similar to the simulations of continuous charging and discharging shown in Figures 4–6. Of course, because there is a period of time during which a vehicle is left unused after charging is complete, the battery's lifespan more rapidly decreases if a relatively low-capacity battery maintains an overvoltage state. As a result, the voltage of low-capacity Bat #3 approaches the overvoltage protection limit of 4.3 V, and subsequent voltage changes due to temperature variations cause the battery to exceed the overvoltage limit, ultimately leading to a battery fire in the electric vehicle. Therefore, to address this problem, a new cell balancing method must be used in the BMS to suppress the voltage increase in low-capacity Bat #3.

3. Proposed Voltage-Based Realignment Cell Balance

Cell balance can be accomplished at any time by the user. In particular, cell balance during charging requires a lot of attention. When cell balance is performed during charging in a series-connected battery, resistance is connected in parallel to the battery, reducing the total resistance value. This changes the overall voltage distribution value of the series-connected batteries. In the simulation results in Section 2, it is confirmed that a low cell balance current is meaningless. Rather, it causes the problem of increasing the highest voltage of a battery with a relatively small capacity. In this section, the authors investigate a new cell balance method to solve the problem without changing any hardware.

3.1. Proposed New Cell Balance Method to Prevent Overvoltage Due to Aging

In previous studies, a cell balancing method was proposed to make the SOC of all cells 100% when charging was complete [7]. However, this method can put a heavy burden on the BMS, as it requires the individual calculation of the SOC of all series-connected batteries. Therefore, in this study, a method using only the voltage is proposed to solve the problem of the maximum voltage rising due to aging. Table 5 shows that Bat #3 with the minimum capacity determines the charge–discharge current, and it can be seen that it quickly approaches overvoltage as the aging relatively quickly progresses. In addition, it is confirmed that the voltage rise of the average capacity battery suppresses the maximum voltage rise of a relatively small-capacity battery. Figure 9 shows the cell balance flow chart of the new method. Initially, the full charge and full discharge are slow-charging and without cell balancing. Measuring the highest voltage of each battery and setting the measured voltage as the reference for the cell balance voltage allows for the highest voltage of a battery to have a relatively small capacity, which is applied as the cell balance reference voltage of the remaining batteries. It is applied as the cell balance reference voltage of a relatively small-capacity battery. The reference voltage for the cell balancing of the remaining batteries is set to the highest voltage. The proposed new cell balancing method suggests low-voltage charging for batteries with a relatively low capacity. This slows down the aging process of low-capacity batteries, resulting in a slower increase in the maximum voltage. Additionally, starting from a lower maximum voltage point also slows down the time it takes to reach overvoltage. Cell balancing is performed only at voltages higher than the reference voltage, so the remaining batteries, excluding those with a relatively low capacity, have a relatively high SOC value at the end of charging, which balances the aging rate.

3.2. Simulation Verification of the Proposed Cell Balance

In this section, the potential difference realignment passive balancing method proposed above is simulated. The simulation configuration is configured as shown in Figure 10. The basic conditions are the same as in the previous simulations. However, since the conditions for Charts #1, #2, #3, and #4 are modified, the modified conditions for each simulation are set by taking the initial voltage from the series-connected batteries in Tables 1–4, respectively.

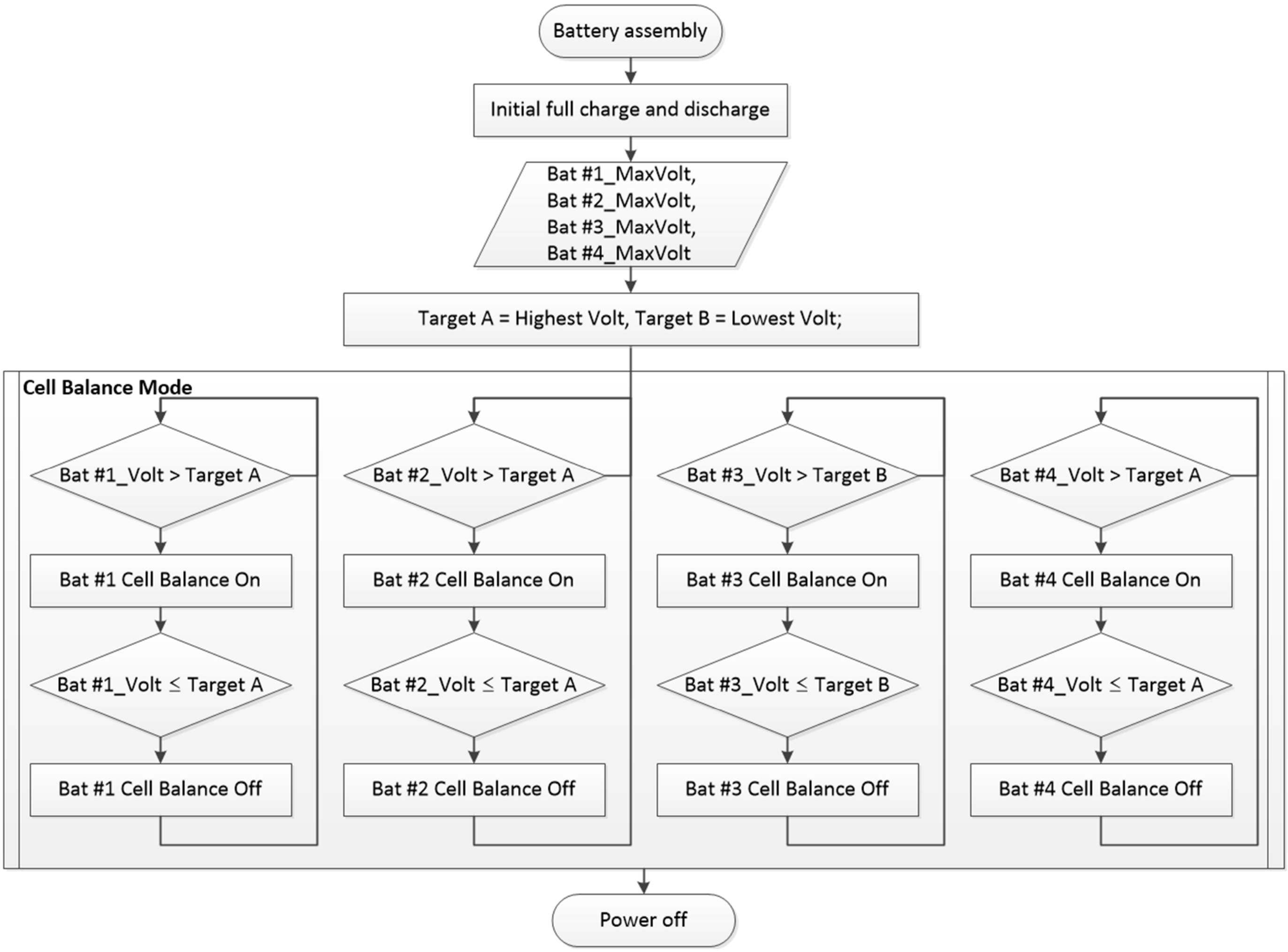

Figure 9. Proposed voltage reference realignment manual cell balance method flowchart.

Simulation Results with Proposed Cell Balancing Implementation

Simulations were performed by applying the proposed cell balance method when the allowable capacity deviation of series-connected batteries was ±1%. Figure 10 shows each chart. Taking the voltage result of the battery from Table 1, applying it to the cell balance reference voltage, and, in the case of battery 3 having a relatively small capacity, the lowest voltage was applied as a standard for cell balance. Batteries 1, 2, and 4 applied the highest voltage as a standard for cell balance. Different charge rates resulted in differences in the DCIR. The difference in the DCIR affected the voltage distribution during charging. Therefore, it suppressed the peak voltage of a relatively small-capacity battery and suppressed the aging rate at the same time.

Figure 11 shows the simulation results. Figure 11a is the simulated voltage result. Figure 11b is the result of extending the voltage of the simulated voltage result from 4.0 V to 4.35 V. Figure 11c is the simulated SOC result. Figure 11d is the simulated SOH result. In Figure 11b, it can be seen that the highest voltage of Bat #3 rises while charging and discharging is repeated. However, after 10×10^6 s, the highest voltage of Bat #3 is lower than in Table 2 because the cell balance reference voltage was lowered.

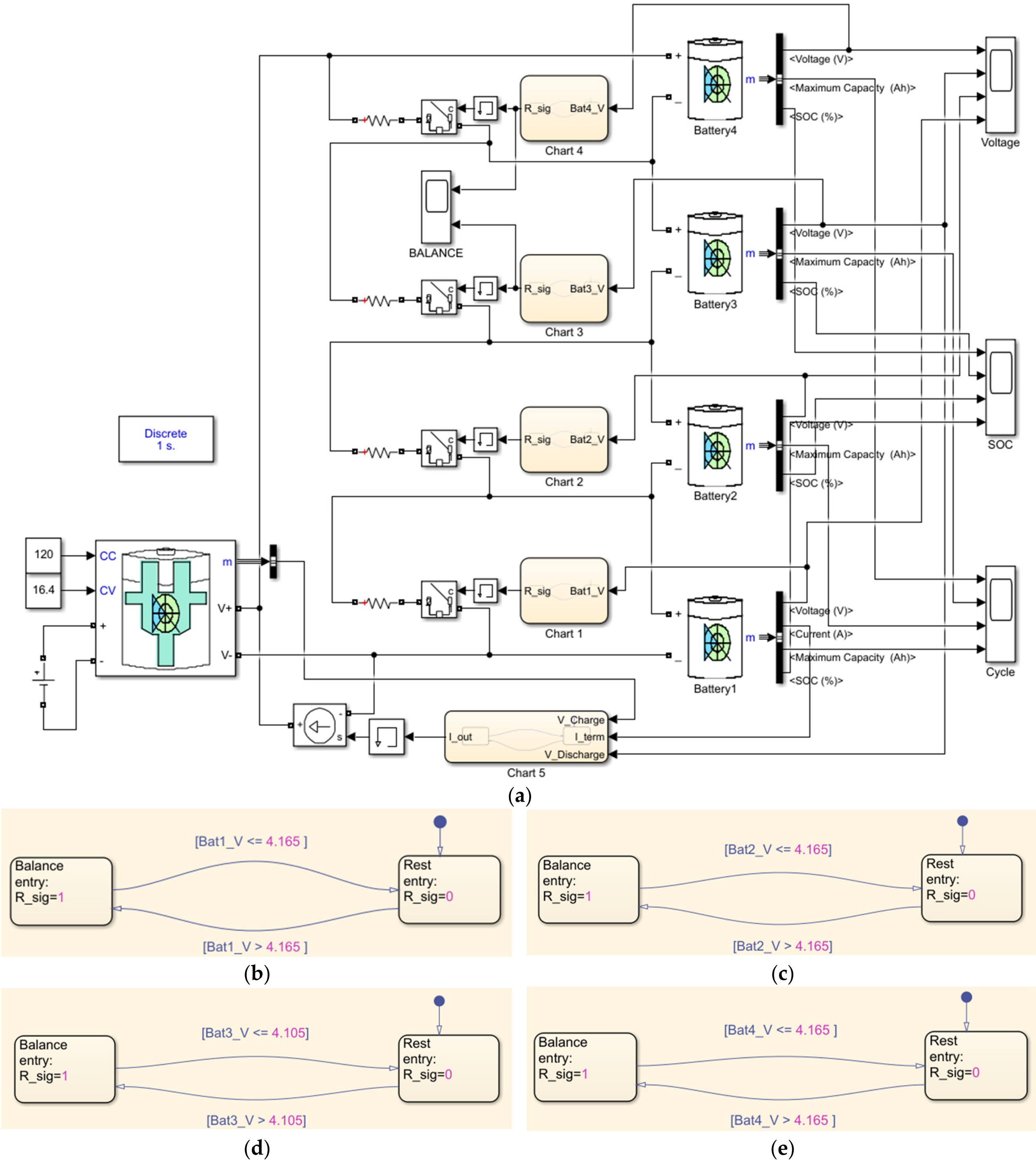

Figure 10. Serial battery aging simulation applying the proposed cell balance. (**a**) Model; (**b**) Stateflow of Chart #1; (**c**) Stateflow of Chart #2; (**d**) Stateflow of Chart #3; (**e**) Stateflow of Chart #4.

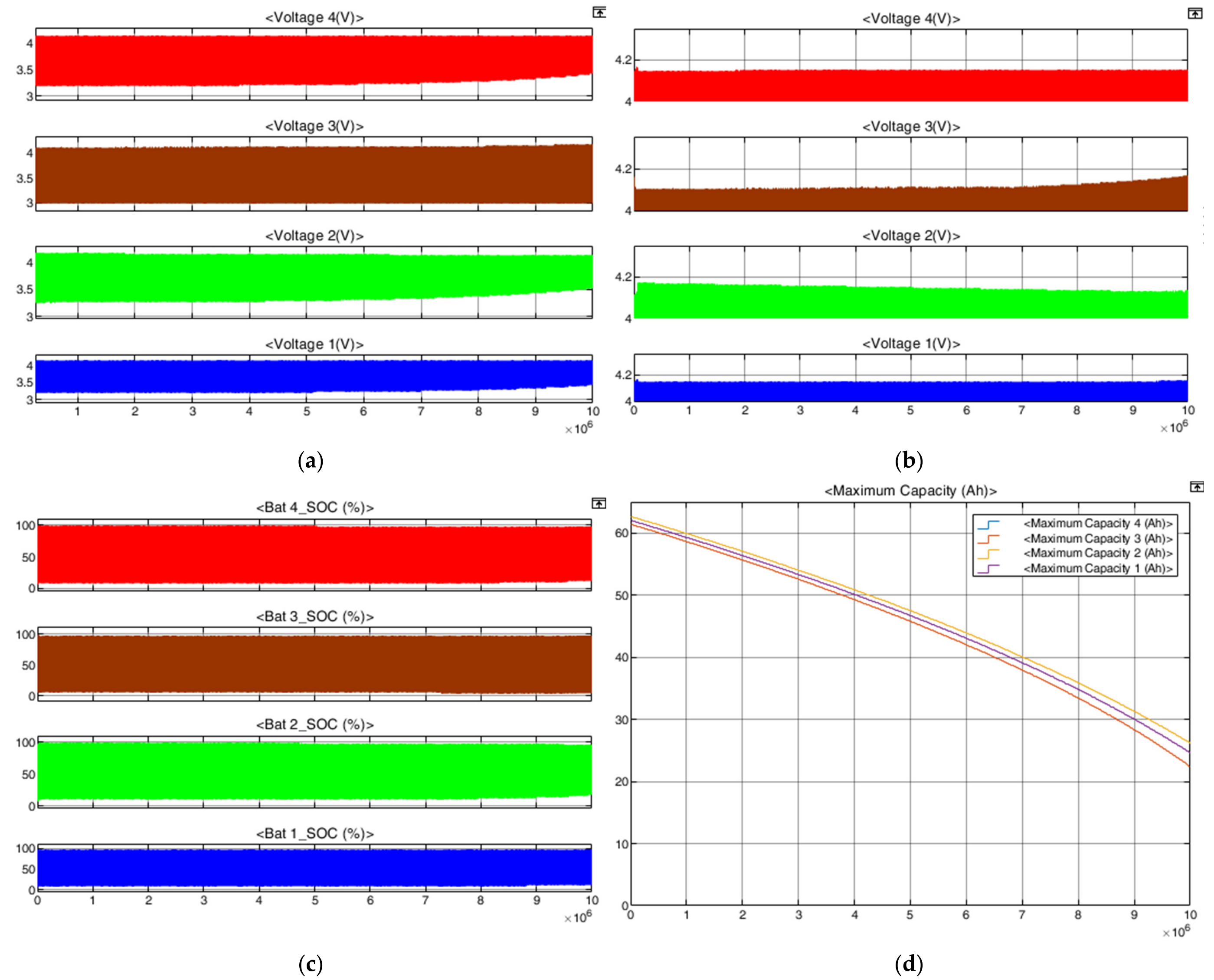

Figure 11. Aging simulation of the proposed cell balance with allowable capacity deviation of ±1%. (**a**) Voltage result; (**b**) magnified voltage result; (**c**) SOC result; (**d**) SOH result.

Table 9 summarizes the simulation results for Figure 11, considering the allowable capacity deviation of ±2% and ±3% in the serially connected battery. In the case of a ±1% allowable capacity deviation, the highest voltage of Bat #3 is 4.167 V; in the case of a ±2% deviation, it is 4.093 V; and, in the case of a ±3% deviation, it is 4.049 V. This proves that the prevention of the highest voltage of a relatively smaller battery from approaching the OVP voltage is achieved.

Table 9. Comparison of simulation results when cell balance cell balancing.

For 10 × 10^6 s

Parameter		Capacity Deviation of ±1%				Capacity Deviation of ±2%				Capacity Deviation of ±3%			
		Bat #1	**Bat #2**	**Bat #3**	**Bat #4**	**Bat #1**	**Bat #2**	**Bat #3**	**Bat #4**	**Bat #1**	**Bat #2**	**Bat #3**	**Bat #4**
Voltage (V)	Min	3.048	3.086	2.997	3.048	3.086	3.151	2.996	3.086	3.121	3.207	2.997	3.121
	Max	4.129	4.105	4.163	4.129	4.127	4.102	4.201	4.127	4.115	4.099	4.241	4.115
SOC (%)	Min	6.97	7.40	6.43	6.97	7.48	8.31	6.50	7.48	8.00	9.22	6.58	8.00
	Max	98.01	97.54	98.46	98.01	97.91	96.97	98.85	97.91	97.76	96.37	99.19	97.76
SOH (Ah)	Max	62.04	62.66	61.42	62.04	62.04	63.28	60.80	62.04	62.04	63.90	60.18	62.04
Time (Cycles)		1 Cycle				1 Cycle				1 Cycle			
Voltage (V)	Min	3.425	3.518	2.991	3.425	3.610	3.654	2.985	3.610	3.720	3.732	2.989	3.720
	Max	4.151	4.126	4.167	4.151	4.177	4.153	4.093	4.177	4.210	4.211	4.049	4.210
SOC (%)	Min	12.55	17.11	4.31	12.55	25.81	32.11	4.31	25.81	52.97	54.11	4.60	52.97
	Max	96.27	95.75	96.40	96.27	97.16	96.87	93.25	97.16	98.41	97.97	71.41	97.41
SOH (Ah)	Max	24.57	26.16	22.34	24.57	27.34	30.12	21.93	27.34	34.85	37.82	23.70	34.85
Time (Cycles)		4219 Cycles				4454 Cycles				5367 Cycles			

4. Results of the Existing Cell Balance and the Proposed Cell Balance

In Table 10, the authors compare the simulation results of the voltage-based cell balance method and the proposed voltage-based realigned cell balance method. For all the results, the proposed cell balance method showed a higher voltage rise than the voltage-based cell balance method, except for batteries with relatively small capacities. On the contrary, it was possible to be safe from a fire due to overvoltage by suppressing the voltage rise of a battery with a relatively small capacity as much as possible, such that it did not reach overvoltage. In the case of the SOC, it can be confirmed that the proposed cell balance method reduced the overall usage range, which suppressed the SOC range expansion of Bat #3. Therefore, it was confirmed that the deterioration of the battery as a whole was slowed down.

Table 10. Comparison of simulation results when cell balance is adjusted based on a simple voltage difference and when the proposed voltage-based reordering cell balancing method is applied.

For 10 × 10^6 s

Parameter		Bat #1	Bat #2	Bat #3	Bat #4
Volt. ref. cell balance with capacity deviation ±1%	Max. Volt.	↑ 0.015 V	↑ 0.023 V	↑ 0.048 V	↑ 0.015 V
	SOC Use	91.04% → 87.16%	90.15% → 82.25%	92.03% → 93.16%	91.04% → 87.16%
	SOH	↓ 62.06%	↓ 60.20%	↓ 64.15%	↓ 62.06%
	Cycles	4176 Cycles			
Proposed cell balance with capacity deviation ±1%	Max. Volt.	↑ 0.022 V	↑ 0.021 V	↑ 0.004 V	↑ 0.022 V
	SOC Use	91.04% → 83.72%	91.11% → 78.64%	92.03% → 92.09%	91.04% → 83.72%
	SOH	↓ 60.40%	↓ 58.25%	↓ 63.63%	↓ 60.40%
	Cycles	4219 Cycles			
Volt. ref. cell balance with capacity deviation ±2%	Max. Volt.	↑ 0.008 V	↑ 0.011 V	↑ 0.072 V	↑ 0.008 V
	SOC Use	90.50% → 82.40%	88.67% → 74.11%	92.35% → 94.14%	90.50% → 82.40%
	SOH	↓ 61.07%	↓ 57.60%	↓ 65.25%	↓ 61.07%
	Cycles	4226 Cycles			
Proposed cell balance with capacity deviation ±2%	Max. Volt.	↑ 0.050 V	↑ 0.051 V	↓ 0.108 V	↑ 0.050 V
	SOC Use	90.43% → 71.35%	88.66% → 64.76%	92.35% → 88.94%	90.43% → 71.35%
	SOH	↓ 55.93%	↓ 52.40%	↓ 63.93%	↓ 55.93%
	Cycles	4454 Cycles			
Volt. ref. cell balance with capacity deviation ±3%	Max. Volt.	↑ 0.008 V	↑ 0.016 V	↑ 0.088 V	↑ 0.008 V
	SOC Use	89.84% → 77.48%	87.16% → 67.03%	92.61% → 95.10%	89.84% → 77.48%
	SOH	↓ 59.25%	↓ 55.38%	↓ 66.62%	↓ 59.25%
	Cycles	4296 Cycles			
Proposed cell balance with capacity deviation ±3%	Max. Volt.	↑ 0.095 V	↑ 0.112 V	↓ 0.192 V	↑ 0.095 V
	SOC Use	89.77% → 45.44%	87.15% → 41.86%	92.61% → 66.81%	89.77% → 45.44%
	SOH	↓ 43.83%	↓ 40.81%	↓ 60.62%	↓ 43.83%
	Cycles	5516 Cycles			

The simulation results of the cell balance method proposed in Table 11 and the cell balance method of the existing simple voltage comparison method are summarized here. For the existing simple voltage comparison cell balancing method, the maximum voltage of the battery greatly increased from 4.213 V to 4.331 V as the allowable capacity deviation of the series-connected batteries increased. However, in the case of the proposed cell balance method, the highest voltage rose from 4.167 V to 4.211 V, which was relatively very small. In addition, for the existing simple voltage comparison cell balance method, it was confirmed that as the allowable capacity deviation of series-connected batteries increased, the aging of batteries with relatively small capacities more quickly proceeded. However, in the case of the proposed cell balance method, the aging and the aspect of the battery were different. This was because the use area of a battery with a relatively small capacity is limited according to the allowable capacity deviation of the battery.

Table 11. Comparison of simulation results of the cell balance method of the existing simple voltage comparison method and the proposed cell balance method.

For 10×10^6 s

Condition	Max. Volt.	Max. Aging Progress
Volt. ref. cell balance with capacity deviation ±1%	4.213 V (Bat #3)	64.15% (Bat #3)
Volt. ref. cell balance with capacity deviation ±2%	4.275 V (Bat #3)	65.25% (Bat #3)
Volt. ref. cell balance with capacity deviation ±3%	4.331 V (Bat #3)	66.62% (Bat #3)
Proposed cell balance with capacity deviation ±1%	4.167 V (Bat #3)	63.63% (Bat #3)
Proposed cell balance with capacity deviation ±2%	4.177 V (Bat #1, #4)	63.93% (Bat #3)
Proposed cell balance with capacity deviation ±3%	4.211 V (Bat #2)	60.62% (Bat #3)

5. Conclusions

The authors understand too little about batteries. S.-S.Y. has been developing Battery Management System (BMS) hardware since 2009, but, as the use cases of batteries have expanded, more questions have arisen; therefore, this study was conducted by organizing the knowledge so far. Batteries can more efficiently use depleted energy, and, even if alternative energy is discovered, efficient operation requires the necessary technology. The authors believe that deeper research into these fundamental technologies will open up a beautiful future for our descendants. The authors conclude that a battery with a relatively small capacity due to gradual damage gradually increases in voltage, and the activity of chemical reactions increases due to a rise in the thermal energy caused by a temperature change, resulting in a rise in the highest voltage, exceeding the protection voltage of the BMS, and causing a battery fire. At this time, the voltage change for the thermal energy of the battery is affected by the SOC–OCV curve, so it is assumed that a larger voltage change occurs for the same energy in the range where the voltage or the SOC is high. In the future, the authors plan to conduct battery fire demonstration experiments according to temperature changes under overvoltage conditions and study the possible solutions.

Author Contributions: Conceptualization, S.-S.Y.; methodology, S.-S.Y.; software, S.-S.Y.; validation, S.-S.Y. and S.-C.K.; formal analysis, S.-S.Y.; investigation, S.-S.Y.; resources, S.-S.Y. and S.-C.K.; data curation, S.-S.Y.; writing—original draft preparation, S.-S.Y. and S.-C.K.; writing—review and editing, S.-S.Y. and S.-C.K.; visualization, S.-S.Y.; supervision, S.-C.K.; project administration, S.-S.Y. and S.-C.K.; funding acquisition S.-C.K. All authors have read and agreed to the published version of the manuscript.

Funding: This research was supported by the Ministry of Science and ICT (MSIT), South Korea, under the Grand Information Technology Research Center support program (IITP-2023-2020-0-01462), supervised by the IITP (Institute for Information & communication Technology Planning & evaluation). This work was supported by a National Research Foundation of Korea (NRF) grant funded by the South Korean government (MSIT) (No. 2022R1A5A8026986).

Institutional Review Board Statement: Not applicable.

Informed Consent Statement: Not applicable.

Data Availability Statement: Not applicable.

Conflicts of Interest: The authors declare no conflict of interest.

References

1. Gao, W.; Zheng, Y.; Ouyang, M.; Li, J.; Lai, X.; Hu, X. Micro-Short-Circuit Diagnosis for Series-Connected Lithium-Ion Battery Packs Using Mean-Difference Model. *IEEE Trans. Ind. Electron.* **2019**, *66*, 2132–2142. [CrossRef]
2. Pinto, C.; Barreras, J.V.; Schaltz, E.; Araujo, R.E. Evaluation of Advanced Control for Li-ion Battery Balancing Systems Using Convex Optimization. *IEEE Trans. Sustain. Energy* **2016**, *7*, 1703–1717. [CrossRef]
3. Sertkaya, M.G.; Yilmaz, E.; Sanli, A.E.; Gunli, G. Comparison of power and energy density after full shunting-balancing in serial connected lithium-ion batteries and serial-connected supercapacitors. In Proceedings of the 2015 3rd International Renewable and Sustainable Energy Conference (IRSEC), Marrakech, Morocco, 10–13 December 2015; pp. 1–5. [CrossRef]
4. Iraola, U.; Aizpuru, I.; Gorrotxategi, L.; Segade, J.M.C.; Larrazabal, A.E.; Gil, I. Influence of Voltage Balancing on the Temperature Distribution of a Li-Ion Battery Module. *IEEE Trans. Energy Convers.* **2015**, *30*, 507–514. [CrossRef]
5. Feng, F.; Hu, X.; Liu, K.; Che, Y.; Linc, X.; Jin, G.; Liu, B. A Practical and Comprehensive Evaluation Method for Series-Connected Battery Pack Models. *IEEE Trans. Transp. Electrif.* **2020**, *6*, 391–416. [CrossRef]
6. Lee, J.; Kim, J.-M.; Ryu, K.; Won, C.-Y. Operation Control Algorithm of ESS with High Reliability. In Proceedings of the 2019 22nd International Conference on Electrical Machines and Systems (ICEMS), Harbin, China, 11–14 August 2019; pp. 1–5. [CrossRef]
7. Yun, S.-S.; Kee, S.-C. Effect of Capacity Variation in Series-Connected Batteries on Aging. *Batteries* **2023**, *9*, 22. [CrossRef]
8. He, L.; Yang, Z.; Gu, Y.; Liu, C.; He, T.; Shin, K.G. SoH-Aware Reconfiguration in Battery Packs. *IEEE Trans. Smart Grid* **2018**, *9*, 3727–3735. [CrossRef]
9. Feng, W.; Jiuchun, J.; Weige, Z.; Huiping, G. Research on the charge mode of series-connected batteries. In Proceedings of the 2008 IEEE Vehicle Power and Propulsion Conference, Harbin, China, 3–5 September 2008; pp. 1–5. [CrossRef]
10. Hosseinzadeh, E.; Odio, M.X.; Marco, J.; Jennings, P. Unballanced Performance of Parallel Connected Large Format Lithium Ion Batteries for Electric Vehicle Application. In Proceedings of the 2019 International Conference on Smart Energy Systems and Technologies (SEST), Porto, Portugal, 9–11 September 2019; pp. 1–6. [CrossRef]
11. Kwon, S.; Han, D.; Lee, S.; Song, H.-C.; Kim, J. Voltage deviation analysis for battery pack Aging. In Proceedings of the Power Electronics Conference, Anaheim, CA, USA, 17–21 March 2019; pp. 451–452.
12. Choi, W.; Hong, S. An Experimental Study on the Cell Balancing Parameters for Faulty Cell Detection in a Battery Module. *Batteries* **2022**, *8*, 218. [CrossRef]
13. Zun, C.-Y.; Park, S.-U.; Mok, H.-S. New Cell Balancing Charging System Research for Lithium-ion Batteries. *Energies* **2020**, *13*, 1393. [CrossRef]
14. Yun, S.-S.; Kee, S.-C. Improved Multilevel Multistage Constant-Current Constant-Voltage Superfast Charging of Multiple Cells. *J. Electr. Eng. Technol.* **2022**, *17*, 209–219. [CrossRef]
15. Omariba, Z.B.; Zhang, L.; Sun, D. Review of Battery Cell Balancing Methodologies for Optimizing Battery Pack Performance in Electric Vehicles. *IEEE Access* **2019**, *7*, 129335–129352. [CrossRef]
16. Zhang, Z.; Cheng, X.; Lu, Z.-Y.; Gu, D.-J. SOC Estimation of Lithium-Ion Battery Pack Considering Balancing Current. *IEEE Trans. Power Electron.* **2018**, *33*, 2216–2226. [CrossRef]
17. Gupta, P.P.; Kumar, N.; Nangia, U. Passive Cell Balancing and Battery Charge Controller with CCCV Topology. In Proceedings of the 2022 3rd International Conference for Emerging Technology (INCET), Belgaum, India, 27–29 May 2022; pp. 1–5. [CrossRef]
18. Zhang, Y.; Liu, Z.; Chen, Z. Smart-Leader-Based Distributed Charging Control of Battery Energy Storage Systems Considering SoC Balance. *Batteries* **2023**, *9*, 18. [CrossRef]
19. Yang, R.; Xiong, R.; Shen, W. On-board soft short circuit fault diagnosis of lithium-ion battery packs for electric vehicles using extended Kalman filter. *CSEE J. Power Energy Syst.* **2022**, *8*, 258–270. [CrossRef]
20. Zheng, L.; Zhu, J.; Wang, G. A comparative study of battery balancing strategies for different battery operation processes. In Proceedings of the 2016 IEEE Transportation Electrification Conference and Expo (ITEC), Dearborn, MI, USA, 27–29 June 2016; pp. 1–5. [CrossRef]
21. Liu, Y.-H.; Hsieh, C.-H.; Luo, Y.-F. Search for an Optimal Five-Step Charging Pattern for Li-Ion Batteries Using Consecutive Orthogonal Arrays. *IEEE Trans. Energy Convers.* **2011**, *26*, 654–661. [CrossRef]
22. Ding, X.; Cui, Z.; Cui, N. Connection Fault Diagnosis for Series-connected Lithium-ion Battery Based on Curve Similarity Calculation and Curve Conversion. In Proceedings of the 2022 6th CAA International Conference on Vehicular Control and Intelligence (CVCI), Nanjing, China, 28–30 October 2022; pp. 1–6. [CrossRef]
23. Gong, X.; Xiong, R.; Mi, C.C. Study of the Characteristics of Battery Packs in Electric Vehicles with Parallel-Connected Lithium-Ion Battery Cells. *IEEE Trans. Ind. Appl.* **2015**, *51*, 1872–1879. [CrossRef]
24. Celen, B.; Aras, A.C.; Dohr, M.; Sivaraman, T. Equivalent Circuit Modeling of All-Solid-State Battery by using DC-IR Data. In Proceedings of the 2021 IEEE International Systems Conference (SysCon), Vancouver, BC, Canada, 15 April–15 May 2021; pp. 1–6. [CrossRef]

25. Rizzello, A.; Scavuzzo, S.; Ferraris, A.; Airale, A.G.; Carello, M. Temperature-Dependent Thévenin Model of a Li-Ion Battery for Automotive Management and Control. In Proceedings of the 2020 IEEE International Conference on Environment and Electrical Engineering and 2020 IEEE Industrial and Commercial Power Systems Europe (EEEIC/I&CPS Europe), Madrid, Spain, 9–12 June 2020; pp. 1–6. [CrossRef]
26. Ansean, D.; Garcia, V.; Gonzalez, M.; Viera, J.; Blanco, C.; Antuna, J. DC internal resistance during charge: Analysis and study on $LiFePO_4$ batteries. In Proceedings of the 2013 World Electric Vehicle Symposium and Exhibition (EVS27), Barcelona, Spain, 17–20 November 2013; pp. 1–11. [CrossRef]
27. Zou, Y.; Hu, X.; Ma, H.; Li, S.E. Combined State of Charge and State of Health estimation over lithium-ion battery cell cycle lifespan for electric vehicles. *J. Power Sources* **2015**, *273*, 793–803. [CrossRef]
28. Lim, D.-J.; Kim, J.-G.; Ahn, J.-H.; Kim, D.-H.; Lee, B.-K. A mixed SOC estimation algorithm using enhanced OCV reset and the DCIR iterative calculation reset. In Proceedings of the 2015 9th International Conference on Power Electronics and ECCE Asia (ICPE-ECCE Asia), Seoul, Republic of Korea, 1–5 June 2015; pp. 1155–1160. [CrossRef]
29. Wang, Q.-K.; He, Y.-J.; Shen, J.-N.; Hu, X.-S.; Ma, Z.-F. State of Charge-Dependent Polynomial Equivalent Circuit Modeling for Electrochemical Impedance Spectroscopy of Lithium-Ion Batteries. *IEEE Trans. Power Electron.* **2018**, *33*, 8449–8460. [CrossRef]
30. El Mejdoubi, A.; Chaoui, H.; Gualous, H.; Bossche, P.V.D.; Omar, N.; Van Mierlo, J. Lithium-Ion Batteries Health Prognosis Considering Aging Conditions. *IEEE Trans. Power Electron.* **2019**, *34*, 6834–6844. [CrossRef]
31. Wang, Q.; Qi, W. New SOC estimation method under multi-temperature conditions based on parametric-estimation OCV. *J. Power Electron.* **2020**, *20*, 614–623. [CrossRef]
32. Huang, S.-C.; Tseng, K.-H.; Liang, J.-W.; Chang, C.-L.; Pecht, M.G. An Online SOC and SOH Estimation Model for Lithium-Ion Batteries. *Energies* **2017**, *10*, 512. [CrossRef]
33. Choi, S.S.; Lim, H.S. Factors that affect cycle-life and possible degradation mechanisms of a Li-ion cell based on $LiCoO_2$. *J. Power Sources* **2002**, *111*, 130–136. [CrossRef]
34. Wang, Q.; Jiang, Y.; Lu, Y. State of Health Estimation for Lithium-ion Battery Based on D-UKF. *Int. J. Hybrid Inf. Technol.* **2015**, *8*, 55–70. [CrossRef]
35. Chen, Y.; Wang, W.; Pagliari, D.J.; Macii, E.; Poncino, M. Assessing the Dependence of Li-Ion Batteries Capacity on Load Current Frequency. In Proceedings of the 2022 International Symposium on Power Electronics, Electrical Drives, Automation and Motion (SPEEDAM), Sorrento, Italy, 22–24 June 2022; pp. 58–63. [CrossRef]
36. Noh, T.-W.; Han, H.-C.; Lee, B.K. An Online State-of-Health Estimation Algorithm for Electric Vehicles through Aging Tendency of Open Circuit Voltage. In Proceedings of the 2019 10th International Conference on Power Electronics and ECCE Asia (ICPE 2019-ECCE Asia), Busan, Republic of Korea, 27–30 May 2019; pp. 1–6. [CrossRef]
37. Xiong, R.; Zhang, Y.; Wang, J.; He, H.; Peng, S.; Pecht, M. Lithium-Ion Battery Health Prognosis Based on a Real Battery Management System Used in Electric Vehicles. *IEEE Trans. Veh. Technol.* **2019**, *68*, 4110–4121. [CrossRef]
38. Tseng, K.-H.; Liang, J.-W.; Chang, W.; Huang, S.-C. Regression Models Using Fully Discharged Voltage and Internal Resistance for State of Health Estimation of Lithium-Ion Batteries. *Energies* **2015**, *8*, 2889–2907. [CrossRef]
39. Jang, H.-J.; Song, T.-S.; Kim, J.-Y.; Kim, S.-J.; Jang, T.-H. Study on Analysis of Fire Factor and Development Direction of Standard/safety Requirement to Keep Safety for Energy Storage System (ESS). *Soc. Stand. Certif. Saf.* **2019**, *9*, 25–49. [CrossRef]
40. Yun, S.-S.; Kee, S.-C. Analysis of the Cell Balancing Effect on the ESS Fire by Simulating the Euljiro 3-ga Subway ESS. *Trans. Korean Inst. Power Electron.* **2020**, *25*, 219–226.
41. Kim, S.-K.; Choi, S.-G.; Jin, S.-Y.; Bang, S.-S. An Experimental Study on Fire Risks Due to Overcharge and External Heat of ESS Lithium Battery. *J. Korean Inst. Fire Sci. Eng.* **2019**, *33*, 59–69. [CrossRef]
42. Lee, S.; Kim, J.; Ha, M.; Song, H. Inrush Current Estimation for Hot Swap of the Parallel Connected Large Capacity Battery Pack. In Proceedings of the 2018 IEEE Energy Conversion Congress and Exposition (ECCE), Portland, OR, USA, 23–27 September 2018; pp. 2489–2492. [CrossRef]
43. Wang, Z.; Davidson, J.N.; Foster, M.P. A large-scale battery energy storage system simulation tool for studying cell variation. In Proceedings of the 10th International Conference on Power Electronics, Machines and Drives (PEMD 2020), Online, 15–17 December 2020; pp. 261–265. [CrossRef]
44. Lu, R.; Zhu, C.; Tian, L.; Wang, Q. Super-Capacitor Stacks Management System with Dynamic Equalization Techniques. *IEEE Trans. Magn.* **2007**, *43*, 254–258. [CrossRef]
45. Kee, S.-C.; Yun, S.S. Energy Storage System Safety Operation Plan by Preventing Overcharge during Relaxation Time. *J. Electr. Eng. Technol.* **2021**, *16*, 1941–1953. [CrossRef]
46. Lai, X.; Yao, J.; Jin, C.; Feng, X.; Wang, H.; Xu, C.; Zheng, Y. A Review of Lithium-Ion Battery Failure Hazards: Test Standards, Accident Analysis, and Safety Suggestions. *Batteries* **2022**, *8*, 248. [CrossRef]
47. Yang, X.; Ma, E.W.M.; Pecht, M. Cell balancing technology in battery packs. In Proceedings of the 2012 13th International Conference on Electronic Packaging Technology & High Density Packaging, Guilin, China, 13–16 August 2012; pp. 1038–1041. [CrossRef]
48. Ye, M.; Song, X.; Xiong, R.; Sun, F. A Novel Dynamic Performance Analysis and Evaluation Model of Series-Parallel Connected Battery Pack for Electric Vehicles. *IEEE Access* **2019**, *7*, 14256–14265. [CrossRef]

49. Perisoara, L.A.; Guran, I.C.; Costache, D.C. A Passive Battery Management System for Fast Balancing of Four $LiFePO_4$ Cells. In Proceedings of the 2018 IEEE 24th International Symposium for Design and Technology in Electronic Packaging (SIITME), Iasi, Romania, 25–28 October 2018; pp. 390–393. [CrossRef]
50. Wu, K.; Wang, H.; Wang, S. A passive balancing algorithm for multi-cells. In Proceedings of the 2022 IEEE International Conference on Integrated Circuits, Technologies and Applications (ICTA), Xi'an, China, 28–30 October 2022; pp. 1–2. [CrossRef]
51. Yun, S.S.; Kee, S.-C. Relaxation Time for Temperature Change of Lithium Ion Battery. In Proceedings of the KSAE 2019 Annual Spring Conference, Berlin, Germany, 16–17 May 2019; pp. 1148–1154.